

Impact of Ground Granulated Blast-Furnace Slag and Reservoir Size on Corrosion in Reinforced Concrete

Kazi Naimul Hoque^{1,*}, Francisco Presuel-Moreno², and Hariharan Balasubramanian³

¹Department of Naval Architecture and Marine Engineering, Bangladesh University of Engineering and Technology (BUET), Dhaka, Bangladesh

²Department of Ocean and Mechanical Engineering, Florida Atlantic University (FAU), Dania Beach, Florida, USA

³Department of Naval Architecture and Marine Engineering, State University of New York Maritime College, Bronx, New York, USA

Email: kazinaim@name.buet.ac.bd (K.N.H.); fpresuel@fau.edu (F.P.-M.);

hbalasubramanian@sunymaritime.edu (H.B.)

*Corresponding author

Abstract—This study investigates the impact of using 50% Ground Granulated Blast-Furnace Slag (GGBS) as a cement replacement on corrosion resistance and compares different measurement techniques for assessing corrosion. Electromigration method was employed to simulate chloride-induced corrosion in RC samples with GGBS. The study used Electrochemical Impedance Spectroscopy (EIS), Linear Polarization Resistance (LPR), and Galvanostatic Pulse (GP) measurements to monitor corrosion current (I_{corr}) over time. Results show that LPR generally indicates higher and more variable I_{corr} values compared to GP, which tends to provide more stable readings. The size of the chloride solution reservoir also affects corrosion rates, with larger reservoirs leading to higher I_{corr} due to increased chloride availability. The findings emphasize the vital impact of measurement methods and experimental settings on assessing concrete reinforcement durability, underscoring the importance of comprehensive evaluation strategies to accurately characterize corrosion behaviour.

Keywords—reservoir lengths, slag, electromigration, concrete solution resistance, corrosion current

I. INTRODUCTION

In temperate, and marine environments, steel reinforcement corrosion is a key factor in the deterioration of reinforced concrete (RC) structures. If not addressed, it leads to issues like reduced steel cross-section, weakened steel-concrete bonds, and a shortened service life for RC structures. Chloride-induced corrosion is the most common, though carbonation can also cause corrosion. Due to the slow progression of corrosion, collecting Valuable Data is challenging, and limited research on corrosion initiation and propagation further complicates understanding, as significant damage takes time to develop [1–3].

Research shows that using cement replacement materials like fly ash, silica fume, and blast-furnace slag can significantly reduce steel corrosion and improve concrete permeability [4, 5]. Silica fume, in particular, enhances durability, while fly ash and slag are commonly used in Korea, despite their high cost and low workability. Torii found that 50% Ground Granulated Blast-Furnace Slag (GGBS) concrete offers similar resistance to chloride penetration as 10% silica fume concrete [6].

Accelerated corrosion tests are widely used to simulate steel corrosion in RC structures, allowing for the assessment of damage like bond loss, cover cracking, and reduced stiffness [7–12]. These tests provide faster insights into the effects of corrosion, such as depassivation, compared to natural corrosion. Studies have explored factors like corrosion initiation, damage progression, and their effects on deformation, ductility, bond strength, and failure modes [13–16]. Current research seeks to shorten the corrosion initiation phase while closely replicating natural corrosion processes, with the aim of reducing overall damage.

In this study, 50% of the cement in the concrete mix was replaced with blast-furnace slag. The length of the anode was adjusted based on the size of the solution reservoir, and chloride transport into the concrete was accelerated by electromigration. This method was developed based on previous research findings [17]. Typically, rebar corrosion begins after a few weeks or months. Corrosion propagation was monitored using Electrochemical Impedance Spectroscopy (EIS), Linear Polarization Resistance (LPR), and Galvanostatic Pulse (GP) measurements.

II. EXPERIMENTAL DETAILS

In April 2016, reinforced concrete samples using a binary mix with Slag (SL) were prepared with a water-to-cement ratio of 0.41. The concrete mix details are provided

in Table I, with further specifics in Appendix 2 of reference [18]. Rebar segments were cut to size, wire-brushed, and cleaned with hexane to remove grease. Each rebar measured 30.5 cm × 12.7 cm × 7.6 cm, had a 0.47 cm radius with #3 rebars, and was drilled and tapped to attach a stainless steel screw for electrical contact, allowing corrosion monitoring. Eleven rebar specimens were cast with a 0.75 cm concrete cover.

During casting, stainless steel or titanium mixed metal oxide (TiMMO) mesh was embedded on the top side of

each specimen, which later became the bottom surface. This mesh, ranging from 2.5 cm to 17.5 cm in length and about 3 cm wide, was positioned along the central portion of the rebar to accelerate chloride transport. The specimens were produced at the Florida Department of Transportation's State Materials Office (FDOT- SMO) and were moved to the fog room for curing after the molds were removed.

TABLE I. CONCRETE MIX DETAIL FOR SL SPECIMENS

Mix	Cementitious Content	Cement Content	50% Slag	Fine agg.	Coarse agg.	w/cm ratio
	(kg/m ³)	(kg/m ³)	(kg/m ³)	(kg/m ³)	(kg/m ³)	
SL	390	195	195	782	1009	0.41

After about a month of high humidity storage at FDOT-SMO, the samples were transferred to FAU SeaTech around late May 2016. At FAU-SeaTech, the samples were kept in a high humidity chamber until the solution reservoirs were installed. The samples were then moved to a laboratory environment (65% RH and 21°C), where plastic reservoirs were attached to the top surface using marine adhesives. These reservoirs, installed 40 days post-casting, were filled with a 10% NaCl solution (by weight) to control the corroding length by adjusting the reservoir size. Reservoir lengths ranged from 2.5 cm to 17.5 cm and were centered along the rebar length.

Before filling the reservoirs, the samples were stored in high humidity environment for 3 to 7 days. Electrodes, matching the size of those embedded during casting, were placed inside the reservoirs. The specimens were placed in transparent plastic containers, partially submerged in a saturated calcium hydroxide solution with 1 cm of the concrete immersed, resting on a white acrylic mesh to minimize leaching from the concrete.

III. ELECTROMIGRATION

A potential difference between the top and bottom mesh was established using a power supply, creating an electric field that drove chlorides from the solution into the concrete towards the embedded rebar. The electrode in the NaCl solution reservoir was connected to the negative terminal, while the embedded mesh was connected to the positive terminal of the power supply. An acrylic mesh was used in the solution reservoir to prevent direct contact between the titanium mix metal oxide wire mesh and the concrete surface. The experimental setup for electromigration is illustrated in Fig. 1.

Electromigration was performed on each specimen, initially with a 9 V applied potential. When measuring rebar potential against a Saturated Calomel Reference Electrode (SCE), a potential greater than +2V was observed while the electric field was active. After 7 days, the potential was reduced to 3 V. The current applied was calculated based on the voltage drop across a 100-ohm resistor over several days. Rebar potential was monitored in relation to the SCE during system disconnection. Even when disconnected, the rebars were polarized due to ionic current from the applied field. If corrosion had not started,

the applied potential was reactivated after monitoring for up to two hours. The electromigration process continued until the rebar potential dropped to -0.150 V_{sce} or more negative, indicating potential corrosion initiation, as reported [17].

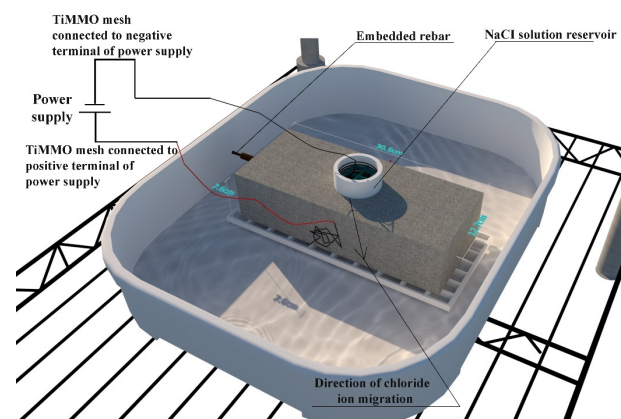


Fig. 1. Experimental setup used for electromigration.

Table II provides the labeling details for each sample, including the sample name/ID, reservoir length, and the start and end dates of electromigration. It also includes a column showing the total calculated ampere-hours applied.

TABLE II. SINGLE REBAR SAMPLES MADE WITH SLAG REPLACEMENT

Sample Number	Reservoir Length (cm)	Migration Time Started	Migration Ending Date	Total Ampere Hour
SL-1	17.5	07/29/16	09/05/16	1.701
SL-2	17.5	07/29/16	01/04/17	1.47
SL-3	17.5	07/26/16	08/15/16	3.162
SL-4	2.5	07/26/16	01/10/17	3.66
SL-5	2.5	07/26/16	01/04/17	3.701
SL-6	5	07/26/16	01/04/17	4.016
SL-7	5	07/26/16	01/04/17	2.482
SL-8	5	07/26/16	01/04/17	2.351
SL-9	10	07/26/16	01/04/17	4.282
SL-10	10	07/26/16	01/04/17	2.369
SL-11	10	07/26/16	12/09/16	3.438

IV. ELECTROCHEMICAL MEASUREMENTS

During the corrosion propagation phase, rebar potential was continuously monitored with a SCE. Concrete

solution resistance (R_s) and corrected polarization resistance (R_c) were assessed at least two days after disconnecting the system, with R_c calculated as the difference between apparent polarization resistance and solution resistance. Starting June 2016, EIS and LPR measurements were performed. EIS covered frequencies from 10 kHz to 1 Hz, with 54.51 Hz selected for R_s measurement. LPR tests ranged from 10 mV below to 1 mV above the open circuit potential, and after six months, from the open circuit potential to 8 mV below it, with scan rates of either 0.1 mV/s or 0.05 mV/s.

Rebar potential, EIS, and LPR measurements were taken monthly after the electromigration system was turned off for at least two days. Beginning May 2017, GP tests were introduced as an alternative method to determine R_s and R_c values. A 10 microampere pulse was applied for 200 seconds, initially measuring the open circuit potential before applying the pulse. R_s (GP) was determined from the initial potential with the pulse, while R_c (GP) was calculated from the potential difference after 200 seconds. R_c values from LPR/EIS and GP tests were converted to I_{corr} using the Stern-Geary equation ($I_{corr} = B/R_p$), where R_p is the polarization resistance (referred as R_c) and B is the Stern-Geary coefficient. Based on previous research, a coefficient of 26 mV for active corroding steel was used in this study [19, 20].

V. RESULTS AND DISCUSSION

The following section compares the evolution of I_{corr} obtained from LPR and GP measurements for different single rebar samples cast with SL over time. The I_{corr} plots are prepared from the values measured between June 2016 to May 2019 from LPR method and between May

2017 to October 2020 from GP method. In ease of comparison, specimens with similar reservoir size are compared together.

Fig. 2 shows the time-dependent evolution of I_{corr} for single rebar SL samples (SL-1, SL-2, SL-3) with a 17.5 cm solution reservoir, measured using LPR and GP techniques. The I_{corr} plots from LPR readings reveal a fluctuating trend across samples, with SL-1 ranging from 24.6-84.2 μA , SL-2 from 16.0-43.7 μA , and SL-3 from 20.5-44.5 μA . The SL-3 sample exhibited a sharp I_{corr} decrease after day 860. For GP measurements, SL-1 and SL-2 also fluctuated slightly, with I_{corr} ranging from 16.1-26.6 μA (SL-1) and 19.3-28.7 μA (SL-2). The SL-3 sample showed an initial drop to 6.9 μA on day 405, followed by slight fluctuations and a gradual decline between days 720 and 1160 before recent increases. Therefore, the I_{corr} values from LPR readings were generally higher than those from GP readings.

Fig. 3 presents the time evolution of I_{corr} for single rebar SL samples (SL-4 and SL-5) under a 2.5 cm solution reservoir, as measured by LPR and GP methods. In the LPR plots, SL-4 shows a significant drop in I_{corr} around day 160, with values generally below 10 μA , fluctuating slightly over time and ranging from 0.6-47.5 μA . The SL-5 sample displays a plateau trend between days 190 and 390, with most I_{corr} values under 10 μA and an overall range of 0.5-36.2 μA . The GP measurements reveal minor fluctuations for SL-4, with I_{corr} between 4.2-12.6 μA . The SL-5 sample initially shows a rising I_{corr} trend, peaking at 22.1 μA at day 450, followed by slight fluctuations until day 650 and a gradual decline thereafter. Notably, I_{corr} values from GP remained below 10 μA for both samples starting from day 820.

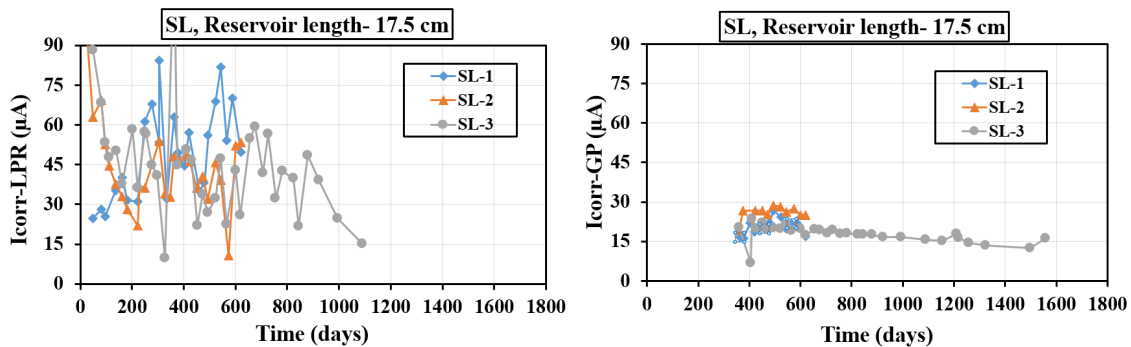


Fig. 2. I_{corr} with time obtained from LPR and GP methods on selected single rebars (SL samples) under 17.5 cm solution reservoir.

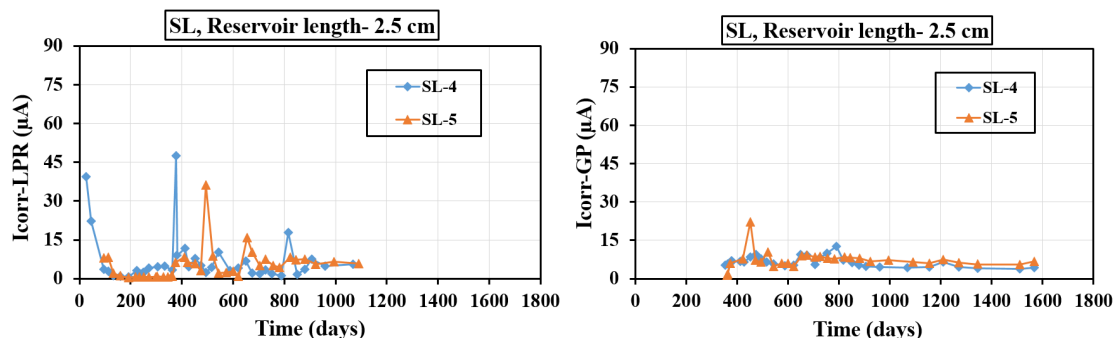


Fig. 3. I_{corr} with time obtained from LPR and GP methods on selected single rebars (SL samples) under 2.5 cm solution reservoir.

Table III summarizes the I_{corr} average and STD values for SL single rebar samples, comparing LPR and GP measurements. The I_{corr} average and STD values were derived from measurements taken between June 2016 and May 2019 using the LPR method, and from May 2017 to October 2020 using the GP method. For samples with a 17.5 cm reservoir length, LPR showed significantly higher I_{corr} averages (49.3 μA , 43.7 μA , 44.5 μA) and STD values (17.6 μA , 16.0 μA , 20.5 μA) than GP, which recorded lower averages (20.5 μA , 25.9 μA , 17.7 μA) and STD values (3.2 μA , 2.5 μA , 3.1 μA). Similarly, for samples with a 2.5 cm reservoir, LPR values remained higher than GP, except for SL-5, where GP averages were slightly higher, and for SL-4, where both methods yielded similar results. Generally, LPR tends to yield higher I_{corr} and greater variability than GP, as it is more sensitive to surface and distribution conditions. A larger reservoir size of 17.5 cm led to higher I_{corr} values compared to the 2.5 cm reservoir, demonstrating that the length of the solution reservoir significantly affects corrosion current. The LPR measures the resistance of a corroding metal surface to small current fluctuations, offering real-time insights into corrosion activity. It typically produces higher I_{corr} values and greater variability because it is sensitive to localized corrosion effects and surface conditions. In contrast, GP

applies a steady current and measures the resulting voltage change, making it less responsive to rapid changes in corrosion activity, which often leads to lower I_{corr} readings. The elevated I_{corr} values from LPR indicate its ability to capture more dynamic corrosion behaviour, especially in environments with higher electrolyte exposure, as seen with the larger reservoir size. The increase in I_{corr} from a 17.5 cm reservoir compared to a 2.5 cm one highlights the significant impact of solution reservoir size on corrosion activity in reinforced concrete structures.

TABLE III. I_{CORR} AVERAGE AND STD VALUES OBTAINED FROM LPR AND GP READINGS FOR SL SINGLE REBAR SAMPLES

Sample Number	Reservoir length (cm)	I_{corr} (average) from LPR (μA)	I_{corr} (STD) from LPR (μA)	I_{corr} (average) from GP (μA)	I_{corr} (STD) from GP (μA)
SL-1*	17.5	49.3	17.6	20.5	3.2
SL-2*		43.7	16.0	25.9	2.5
SL-3		44.5	20.5	17.7	3.1
SL-4	2.5	6.9	9.7	6.5	2.1
SL-5		5.3	6.3	7.3	3.4
SL-6		10.8	8.2	7.4	1.2
SL-7	5	18.2	22.0	10.4	3.7
SL-8		12.9	10.9	14.3	4.8
SL-9		27.3	17.5	10.6	2.3
SL-10	10	28.0	17.9	13.2	3.7
SL-11		36.1	24.4	13.8	5.4

Note: (*) stands for those specimens that have been terminated

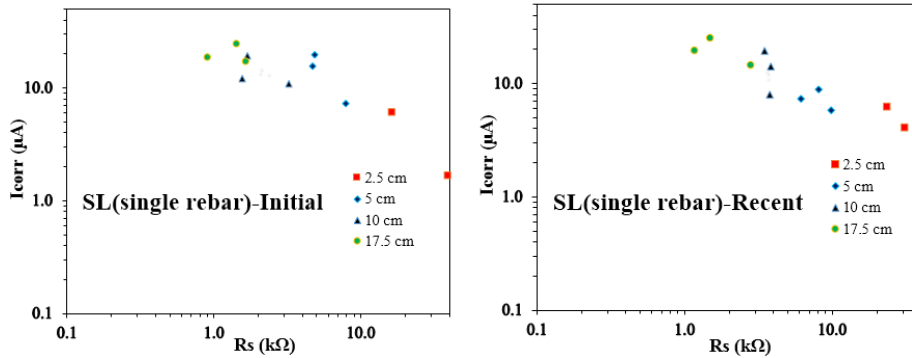


Fig. 4. I_{corr} vs. R_s plot for SL single rebar samples.

Fig. 4 presents I_{corr} vs. R_s plots from GP readings for SL concrete mixes with single rebar samples. The left plot shows initial measurements (May–July 2017), while the right reflects recent data (September–October 2020). The rebars with a 2.5 cm reservoir size exhibited higher R_s values (initial and recent) than other reservoir sizes, with recent I_{corr} values exceeding initial ones. A broader range of I_{corr} values was noted for 5 cm reservoir samples compared to 10 cm, though some I_{corr} values for 5 cm samples were comparable to 10 cm, and 10 cm samples occasionally matched 17.5 cm samples. This suggests similar corroding areas, as corrosion currents were alike. While 17.5 cm reservoir samples had the smallest R_s values, their I_{corr} values were the highest. The initial and recent I_{corr} values demonstrated remarkable consistency across different reservoir sizes. The observed consistency closely aligns with patterns previously reported in the references [21–29].

A detailed summary of Table 3 highlights the I_{corr} average and STD values for SL single rebar samples, with

a comparison between LPR and GP measurement methods, as shown in Fig. 5.

Several factors influence the variations in corrosion current and concrete resistivity values of SL samples measured using LPR and GP techniques. The differences stem from their operational principles: LPR continuously measures polarization resistance, displaying fluctuations in corrosion current, while GP captures a snapshot based on a current pulse response, usually resulting in more stable but lower values.

In marine environments, incorporating slag as a partial substitute for Portland cement in reinforced concrete can greatly improve durability. Slag, a byproduct of steel manufacturing, is rich in reactive silica and calcium, which facilitates the formation of calcium silicate hydrates when mixed with water and calcium hydroxide. This reaction enhances the density of concrete and decreases its permeability, reducing the likelihood of chloride ion intrusion and subsequent corrosion of the steel reinforcements.

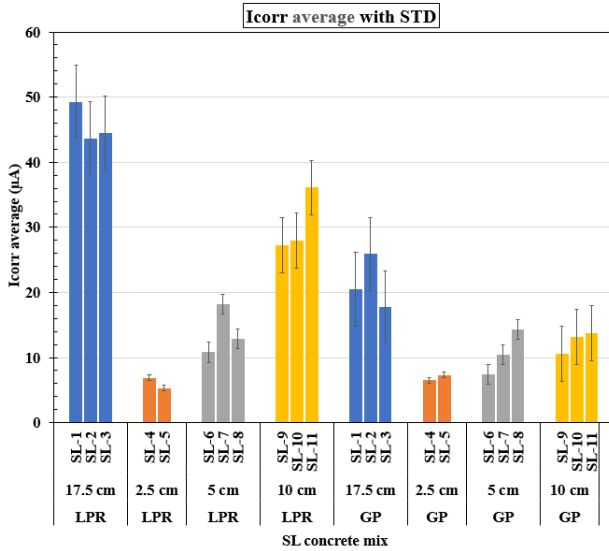


Fig. 5. A summary of Icorr average and STD values obtained from LPR and GP measurements for SL single rebar samples.

Concrete structures, such as bridges and piers, are especially susceptible to high chloride levels in seawater, which heighten the risk of corrosion. Results from LPR and GP measurements show that larger solution reservoirs, mimicking marine conditions, lead to higher Icorr values, indicating that more extensive areas of steel reinforcement may be compromised over time. Fluctuating Icorr values from LPR measurements emphasize the variability of localized corrosion, influenced by temperature, humidity, and chloride exposure. This underscores the necessity for regular monitoring and maintenance of marine infrastructure to prevent unexpected failures and costly repairs.

The study demonstrates that reservoir size impacts corrosion currents: larger reservoirs provide more chloride ions and moisture, leading to increased corrosion activity, while smaller reservoirs limit these agents, resulting in lower Icorr values. Effective corroding areas under different reservoir sizes can yield similar corrosion readings despite varying overall sizes. Grasping the distinct behaviours of LPR and GP methods is essential for understanding corrosion dynamics. LPR captures transient fluctuations due to its sensitivity to surface conditions, while GP offers more stable measurements that might miss rapid changes. Using both techniques provides a comprehensive assessment of corrosion processes.

Structural factors, such as concrete cover quality, moisture retention, and chloride exposure, significantly influence corrosion rates. Structures with inadequate cover or poor maintenance are more susceptible to corrosion, resulting in higher Icorr readings, especially in marine environments. Incorporating slag into concrete mixtures enhances resistance to harsh marine conditions, reducing corrosion risks and extending the lifespan of critical infrastructure. This strategy not only lowers repair frequency but also improves overall safety. The interplay between measurement techniques, slag use, reservoir size, and time in assessing corrosion behaviour underscores the need for careful design and maintenance practices.

VI. CONCLUSION

This investigation into Icorr for SL single rebar samples reveals critical insights into the effects of measurement techniques and reservoir size on corrosion behaviour. While comparing LPR and GP methods, LPR generally yields higher and more variable Icorr values, capturing more pronounced fluctuations, while GP provides more stable readings. The reservoir size strongly impacts corrosion rates, with larger reservoirs (17.5 cm) showing higher Icorr values due to increased chloride availability and larger corroding areas, whereas smaller reservoirs (2.5 cm) reflect reduced corrosion and higher concrete resistivity.

In marine environments, using slag as a partial cement replacement improves concrete durability by creating a denser matrix that limits chloride penetration and lowers corrosion rates, as reflected in reduced Icorr values, especially in smaller reservoir sizes. Similar Icorr values across reservoir sizes suggest that corrosion rates depend on the effective corroding area, highlighting the need to consider measurement techniques and experimental conditions. The interplay between measurement methods, reservoir size, and time is crucial in understanding corrosion behaviour, emphasizing the need for robust evaluation strategies to assess concrete reinforcement durability.

CONFLICT OF INTEREST

The authors declare no conflict of interest.

AUTHOR CONTRIBUTIONS

Kazi Naimul Hoque: Conceptualization, Methodology, Resources, Data curation, Writing-Original draft preparation, Visualization, Investigation, Writing-Reviewing and Editing. Francisco Presuel-Moreno: Conceptualization, Methodology, Writing-Reviewing and Editing, Supervision. Hariharan Balasubramanian: Writing-Reviewing and Editing.

FUNDING

This research is funded through grants provided by Florida Atlantic University, as well as the National Center for Transportation Infrastructure Durability & Life-Extension (TriDurLE), and the Florida Department of Transportation (FDOT).

ACKNOWLEDGEMENT

The authors would like to express their gratitude to the Florida Department of Transportation (FDOT) for their assistance in preparing the samples. The opinions expressed in this paper are those of the authors and not necessarily those of FAU, the FDOT, and TriDurLE.

REFERENCES

- [1] A. Castel, T. Vidal, R. Francois, and G. Arliguie, "Influence of steel-concrete interface quality on reinforcement corrosion induced by chlorides," *Mag. Concr. Res.*, vol. 55, no. 2, pp. 151–160, 2003.

- [2] R. Francois and G. Arliguie, "Influence of service cracking on reinforcement steel corrosion," *J. Mater. Civ. Eng.*, vol. 10, no. 1, pp. 14–20, 1998.
- [3] M. Otieno, H. Beushausen, and M. Alexander, "Chloride-induced corrosion of steel in cracked concrete—part I: Experimental studies under accelerated and natural marine environments," *Cem. Concr. Res.*, vol. 79, pp. 373–385, 2016.
- [4] G. J. Osborne, "Durability of Portland blast-furnace slag cement concrete," *Cem. Concr. Compos.*, vol. 21, pp. 11–21, 1999.
- [5] E. F. Irassar, M. Gonzalez, and V. Rahhal, "Sulphate resistance of type V cements with limestone filler and natural pozzolana," *Cem. Concr. Compos.*, vol. 22, pp. 361–368, 2000.
- [6] K. Torii, T. Sasatani, and M. Kawamura, "Effects of fly ash, blast furnace slag, and silica fume on resistance of mortar to calcium chloride attack," in *Proc. Fifth International Conference on Fly Ash, Silica Fume, Slag, and Natural Pozzolans in Concrete*, American Concrete Institute, SP-153, 1995, vol. 2, pp. 931–949.
- [7] Y. Ballim and J. C. Reid, "Reinforcement corrosion and the deflection of RC beams—an experimental critique of current test methods," *Cement Concr. Compos.*, vol. 25, no. 6, pp. 625–632, 2003.
- [8] T. El Maaddawy and K. Soudki, "A model for prediction of time from corrosion initiation to corrosion cracking," *Cement Concr. Compos.*, vol. 29, no. 3, pp. 168–175, 2007.
- [9] K. N. Hoque, "Analysis of structural discontinuities in ship hull using finite element method," M.Sc. Thesis, Dept. Naval Archit. Mar. Eng., Bangladesh Univ. Eng. Technol. (BUET), Dhaka, Bangladesh, 2016.
- [10] G. Malumbela, P. Moyo, and M. G. Alexander, "Behaviour of reinforced concrete beams under sustained service loads," *Constr. Build. Mater.*, vol. 23, no. 11, pp. 3346–3351, 2009.
- [11] A. A. Torres-Acosta, M. J. Fabela-Gallegos, A. Munoz-Noval, D. Vazques-Vega, and J. R. Hernandez-Jimenez, "Influence of corrosion on the structural stiffness of reinforced concrete beams," *Corrosion*, vol. 60, no. 9, pp. 862–872, 2004.
- [12] A. A. Torres-Acosta, S. Navarro-Gutierrez, and J. Teran-Guillen, "Residual flexure capacity of corroded reinforced concrete beams," *Eng. Struct.*, vol. 29, no. 6, pp. 1145–1152, 2007.
- [13] T. A. El Maaddawy and K. A. Soudki, "Effectiveness of impressed current technique to simulate corrosion of steel reinforcement in concrete," *ASCE J. Mater. Civ. Eng.*, vol. 15, no. 1, pp. 41–47, 2003.
- [14] R. B. Polder and H. A. Peelen, "Characterisation of chloride transport and reinforcement corrosion in concrete under cyclic wetting and drying by electrical resistivity," *Cem. Concr. Compos.*, vol. 24, pp. 427–435, 2002.
- [15] J. Wu, H. Li, Z. Wang, and J. Liu, "Transport model of chloride ions in concrete under loads and drying-wetting cycles," *Constr. Build. Mater.*, vol. 112, pp. 733–738, 2016.
- [16] H. Ye, X. Jin, C. Fu, N. Jin, Y. Xu, and T. Huang, "Chloride penetration in concrete exposed to cyclic drying-wetting and carbonation," *Constr. Build. Mater.*, vol. 112, pp. 457–463, 2016.
- [17] F. Presuel-Moreno, H. Balasubramanian, and Y.-Y. Wu, "Corrosion of reinforced concrete pipes: An accelerated approach," in *Proc. Corrosion 2013*, Houston, TX, USA, 2013, paper no. C2013-0002551.
- [18] F. Presuel-Moreno, M. Nazim, F. Tang, K. Hoque, and R. Bencosme, "Corrosion Propagation of Carbon Steel Rebars in High Performance Concrete," BDV27-977-08 Final Rep., FDOT, 2018.
- [19] V. Feliu, J. A. Gonzalez, and S. Feliu, "Corrosion estimates from transient response to a potential step," *Corros. Sci.*, vol. 49, no. 8, pp. 3241–3255, 2007.
- [20] J. A. Gonzalez, J. M. Miranda, and S. Feliu, "Consideration on the reproducibility of potential and corrosion rate measurements in reinforced concrete," *Corros. Sci.*, vol. 46, no. 10, pp. 2467–2485, 2004.
- [21] K. N. Hoque and F. Presuel-Moreno, "Accelerated Corrosion of Steel Rebar in Concrete by Electromigration: Effect of Reservoir Length and Concrete Mixes," in *Proc. MARTEC 2022*, 2023.
- [22] K. N. Hoque and F. Presuel-Moreno, "Corrosion propagation of steel rebar embedded in marine structures prepared with binary blended concrete containing slag," in *Proc. MARTEC 2022*, 2023.
- [23] K. N. Hoque and F. Presuel-Moreno, "Corrosion behaviour of reinforcing steel embedded in fly ash concrete," in *Proc. MARTEC 2022*, 2023.
- [24] K. N. Hoque and F. Presuel-Moreno, "Corrosion of steel rebar embedded in ternary blended concrete exposed to high humidity environment," in *Proc. MARTEC 2022*, 2023.
- [25] K. N. Hoque, F. Presuel-Moreno, and M. Nazim, "Corrosion of carbon steel rebar in binary blended concrete with accelerated chloride transport," *J. Infrastruct. Preserv. Resil.*, vol. 4, no. 26, 2023.
- [26] K. N. Hoque, F. Presuel-Moreno, and M. Nazim, "Accelerated electromigration approach to evaluate chloride-induced corrosion of steel rebar embedded in concrete," *Adv. Mater. Sci. Eng.*, Art. ID 6686519, 2023.
- [27] K. Hoque, "Corrosion propagation of reinforcing steel embedded in binary and ternary concrete," Ph.D. Dissertation, Dept. Ocean Mech. Eng., Florida Atlantic Univ. (FAU), Boca Raton, FL, USA, 2020.
- [28] F. Presuel-Moreno and K. Hoque, "Corrosion propagation of carbon steel rebar embedded in concrete," in *Proc. Corrosion 2019*, Nashville, TN, USA, 2019.
- [29] F. Presuel-Moreno, K. Hoque, and A. Rosa-Pagan, "Corrosion propagation monitoring using galvanostatic pulse on reinforced concrete legacy samples," 2020-FAU-02 Final Rep., Nat. Univ. Transp. Center TriDurLE, 2022.

Copyright © 2025 by the authors. This is an open access article distributed under the Creative Commons Attribution License which permits unrestricted use, distribution, and reproduction in any medium, provided the original work is properly cited (CC BY 4.0).